Chemical Science

ROYAL SOCIETY OF CHEMISTRY

EDGE ARTICLE

View Article Online
View Journal | View Issue

Cite this: *Chem. Sci.*, 2020, **11**, 4403

All publication charges for this article have been paid for by the Royal Society of Chemistry

Received 24th March 2020
Accepted 1st April 2020

DOI: 10.1039/d0sc01704c

rsc.li/chemical-science

An RGB-emitting molecular cocktail for the detection of bacterial fingerprints†

Sheng Hong, ‡[a] Di-Wei Zheng,‡[a] Qiu-Ling Zhang,[a] Wei-Wei Deng,[b] Wen-Fang Song,[a] Si-Xue Cheng,[a] Zhi-Jun Sun[b] and Xian-Zheng Zhang *[a]

Accumulating evidence indicates that colonized microbes play a crucial role in regulating health and disease in the human body. Detecting microbes should be essential for understanding the relationship between microbes and diseases, as well as increasing our ability to detect diseases. Here, a combined metabolic labeling strategy was developed to identify different bacterial species and microbiota by the use of three different fluorescent metabolite derivatives emitting red, green, and blue (RGB) fluorescence. Upon co-incubation with microbes, these fluorescent metabolite derivatives are incorporated into bacteria, generating unique true-color fingerprints for different bacterial species and different microbiota. A portable spectrometer was also fabricated to automate the colorimetric analysis in combination with a smartphone to conveniently identify different bacterial species and microbiota. Herein, the effectiveness of this system was demonstrated by the identification of certain bacterial species and microbiota in mice with different diseases, such as skin infections and bacteremia. By analyzing the microbiota fingerprints of saliva samples from clinical patients and healthy people, this system was proved to precisely distinguish oral squamous cell carcinoma (OSCC, $n = 29$) samples from precancerous ($n = 10$) and healthy ($n = 5$) samples.

Introduction

The human body is a diverse ecosystem that harbors up to 10^{14} bacterial cells.[1] With our in-depth understanding of the critical relationship between microbes and diseases, the study of commensal microbes is currently in the spotlight.[2–7] For example, *Fusobacterium nucleatum*, a bacterium that exists in the gut, can be viewed as a biomarker for colorectal cancer (CRC) diagnosis.[8] Some specific oral bacteria, including *Capnocytophaga gingivalis*, *Prevotella melaninogenica*, and *Streptococcus mitis*, have been found to predict 80% of oral squamous cell carcinoma (OSCC) cases.[9] Apart from the changes in specific types of bacteria, the occurrence and progression of disease is also accompanied by alteration of the microbial community structure. By using genome sequencing, analysis of the microbial community gives a classification accuracy of 80.3% in identifying CRC patients.[10–12] Considering the close relationship between microbes and diseases, detection methods for microbes should be essential for understanding the interactions of microbes and diseases as well as furthering our ability to detect disease with increasing sophistication.

There are various techniques that have been developed to analyze microbes. Among those, genome sequencing, protein mass spectrum detection, and fluorescence *in situ* hybridization (FISH) are the three most commonly used techniques.[13,14] The first two are superior in their high throughput, but their shortcomings include high cost and complex operation, which largely hinder their pervasive application. Although FISH has been broadly used in cellular imaging and pathogenic diagnosis due to its high sensitivity and satisfactory specificity, it is a tedious procedure with too many false negative results, which limits its application prospects. Additionally, the limitation of using one specific probe for only one bacterial species also greatly restricts its capacity in multiple-bacteria analysis and microbiota identification.[15] Given that the interaction of microbes and diseases is a complex relationship involving diverse bacterial species, it is quite necessary to develop techniques that can not only recognize specific bacterial species, but also identify the distinct fingerprint between different microbiota.

Metabolic labeling, depending on the biosynthetic mechanism to assimilate functionalized metabolites, has recently emerged as a promising method for studying the metabolic processes of living systems.[16–18] Peptidoglycan, one of the major components of bacterial cell walls, is a multi-layer network structure composed of glycans and short peptides, and it has

[a]*Key Laboratory of Biomedical Polymers of Ministry of Education, Department of Chemistry, Wuhan University, Wuhan 430072, P. R. China. E-mail: xz-zhang@whu.edu.cn*

[b]*Department of Oral Maxillofacial Head Neck Oncology, School and Hospital of Stomatology, Wuhan University, Wuhan 430072, P. R. China*

† Electronic supplementary information (ESI) available. See DOI: 10.1039/d0sc01704c

‡ These authors contributed equally to this work.

been labeled to study the synthesis of bacterial cell walls.[19–23] Modified monosaccharides and amino acids have been shown to be incorporated into the peptidoglycan construction without affecting the normal growth, metabolism, or multiplication of bacteria, and have been used to efficiently label bacteria for the purpose of distinguishing them. Specifically, fluorophore-modified D-amino acids have been developed for the metabolic labeling of bacteria.[24–27] In addition, previous studies have reported the labeling of bacteria with derivatives of monosaccharides, such as *N*-acetylmuramic acid, *N*-acetylglucosamine, *N*-acetylgalactosamine, and arabinose.[28–31] However, the metabolic incorporation strategy to use only one functionalized metabolite is imprecise and is insufficient for bacterial recognition in a complex environment such as the microbiota.

Taking these into account, we attempted to develop a strategy to more accurately distinguish specific bacterial species and even different microbiota using a combined metabolic labeling strategy. Based on the fact that the metabolic characteristics vary between bacteria, and different bacterial species incorporate different metabolites for biosynthesis, the labeling of bacteria through the modification of different metabolites with different reporters might be a more effective strategy to distinguish bacteria.

Here, we chose three metabolites, D-amino acids, *N*-acetylglucosamine, and *N*-acetylgalactosamine, that are essential for bacterial biosynthesis and modified them with blue fluorescent coumarin, green fluorescent fluorescein, and red fluorescent rhodamine B, respectively (Fig. 1A). The metabolic incorporation capacity of these metabolite derivatives varies in different bacteria. Thus, different bacteria will incorporate different modified metabolites to exhibit different red, green, and blue (RGB) fluorescence and generate distinguishable true-color patterns that can be used to conveniently and effectively identify different bacterial species or even different microbiota.[32] We also fabricated a portable spectrometer by 3D printing technology to intuitively observe the RGB fluorescence, and be able to directly read the RGB fluorescence values with a commercialized mobile application (App) on a smartphone (coined the "Microcolor system").

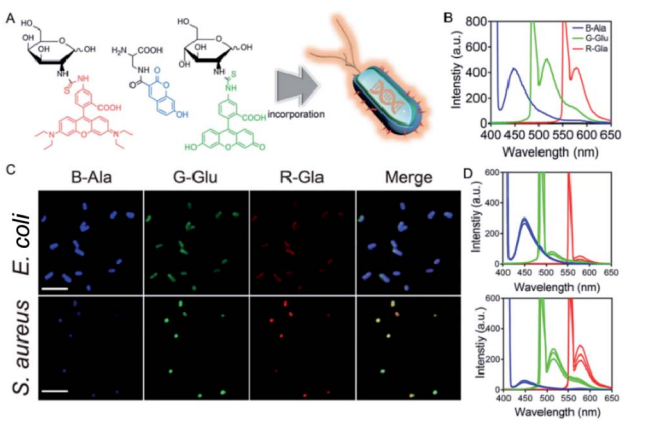

Fig. 1 The combined metabolic labeling strategy. (A) A schematic diagram showing the metabolic incorporation of B-Ala, G-Glu, and R-Gal into bacteria. (B) Fluorescence spectra of the fluorophore-conjugated metabolites. (B-Ala, Ex: 405 nm, Em: 450 nm; G-Glu, Ex: 495 nm, Em: 525 nm; R-Gal, Ex: 555 nm, Em: 590 nm. Ex and Em denote the excitation wavelength and emission wavelength, respectively.) (C) Fluorescence images of fluorophore-conjugated metabolites labeled *E. coli* and *S. aureus* (scale bar: 5 μm). (D) Fluorescence spectra of fluorophore-conjugated metabolites labeled *E. coli* and *S. aureus*. Typical data from at least three independent experiments are presented.

To verify its effectiveness, the efficiency of the Microcolor system in distinguishing different bacterial species was first studied. Samples collected from complex environments (skin infection and bacteremia) were also tested by the Microcolor system to demonstrate its robustness. After that, we extended this strategy to detect diseases that are accompanied by changes in microbiota fingerprints. Saliva specimens of OSCC ($n = 29$), precancerous ($n = 10$) cases, and healthy volunteers ($n = 5$) were analyzed by the Microcolor system to confirm its potential to detect diseases.

Results and discussion

To verify the effectiveness of our combined metabolic labeling strategy, three fluorophore-conjugated metabolites, including blue fluorescent coumarin labeled-alanine (B-Ala), green fluorescent fluorescein labeled-glucose (G-Glu), and red fluorescent rhodamine labeled-galactose (R-Gal), were synthesized. The results from both proton nuclear magnetic resonance (^{1}H-NMR) spectroscopy and electrospray ionization-mass spectrometry (ESI-MS) demonstrated the successful synthesis of these modified metabolites (Fig. S1†). After successfully modifying the metabolites, the fluorescence spectra of the three fluorophore-conjugated metabolites were measured. As shown in Fig. 1B, B-Ala, G-Glu, and R-Gal exhibited characteristic blue, green, and red fluorescence, respectively, under excitation. Then, two common bacterial species, *Escherichia coli* and *Staphylococcus aureus*, were chosen to co-culture with these fluorescent metabolite derivatives to verify whether the modified metabolites could be incorporated into the bacteria as expected.

The fluorescent images in Fig. 1C indicated the successful incorporation of the modified metabolites into the two bacterial species, in which the *E. coli* showed quite strong blue fluorescence and *S. aureus* showed obvious green and red fluorescence. The distinctly different fluorescence characteristics of *E. coli* and *S. aureus* demonstrated the potential of this combined metabolic labeling strategy to distinguish between bacterial species. The fluorescence spectra of the two bacterial species in Fig. 1D also demonstrated the same result. Additionally, whether the labeling procedure would influence the growth of bacteria was also investigated, and it was proved to have no effect on bacterial growth (Fig. S2†).

Furthermore, whether this combined metabolic labeling strategy could specifically label multiple bacteria in a mixed culture system was investigated (Fig. 2A). As shown in Fig. 2B, images from fluorescence microscopy indicated that *Enterococcus faecalis*, *E. coli*, and *Bacillus subtilis* exhibited distinct fluorescence signatures not only in single cultivation but also in mixed cultivation. After labeling, it was observed that *E. faecalis*, *E. coli*, and *B. subtilis* displayed obvious orange, green, and blue

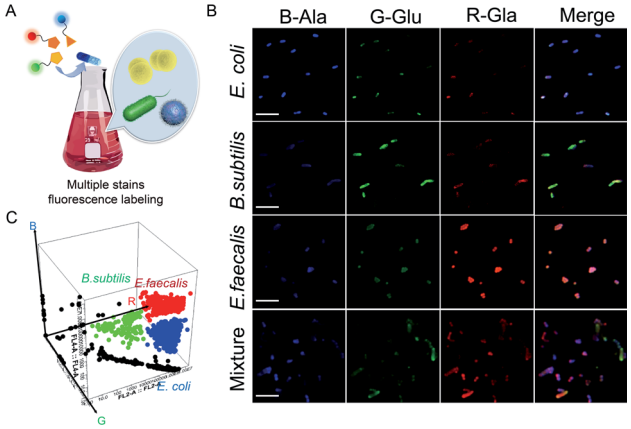

Fig. 2 Combined metabolic labeling strategy in a complex mixture. (A) Combined metabolic labeling strategy for the one-pot labeling of mixed bacteria in a complex mixture. (B) Fluorescence images of fluorophore-conjugated metabolites labeled *E. coli*, *B. subtilis*, and *E. faecalis* and a mixture of the three (scale bar: 5 μm). (C) Flow cytometry for identifying fluorophore-conjugated metabolites labeled *E. coli*, *B. subtilis*, and *E. faecalis* in a mixed culture system. A representative image of three biological replicates is shown.

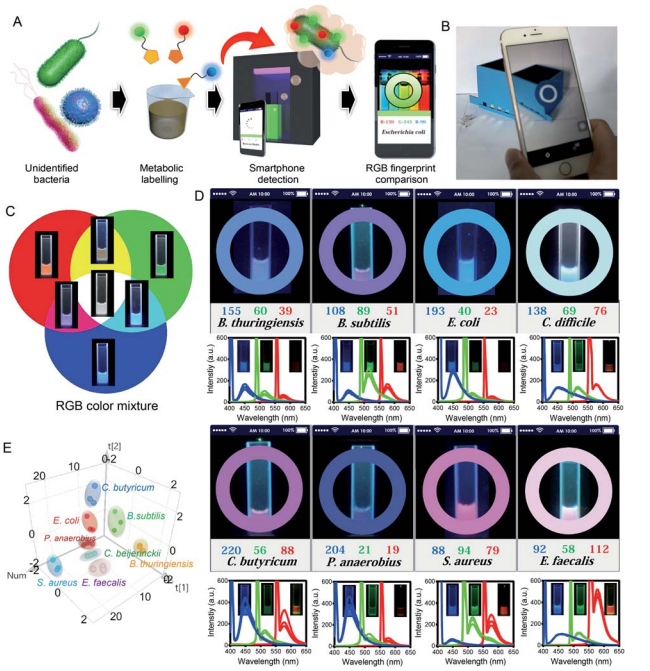

Fig. 3 Labeling of bacteria by the Microcolor system. (A) A schematic diagram showing the use of a 3D-printed portable spectrometer coupled with a smartphone for reading the RGB values of samples. (B) RGB values of samples read with an app on the smartphone. (C) Emission color coordinates of solution mixtures of B-Ala, G-Glu, and R-Gal. (D) Fluorescence fingerprints of eight typical bacteria: *B. thuringiensis*, *B. subtilis*, *E. coli*, *C. difficile*, *C. butyricum*, *P. anaerobius*, *S. aureus*, and *E. faecalis*. Typical data from at least three independent experiments are presented. (E) PCA analysis of the fluorescence fingerprints of the eight different bacteria. The data were obtained from the portable spectrometer. Three biological replicates are shown.

fluorescence, respectively. Even in a triple mixture, the different species could still be accurately identified by their unique fluorescence emission, indicating that this strategy could also specifically label multiple bacteria in a mixed system. Here, flow cytometry was also used to analyze the different bacterial species in a mixed culture system, and the bacteria were also successfully divided into three groups, which was consistent with the result obtained for the combined metabolic labeling strategy (Fig. 2C). Different bacterial species in a complex mixture were separately labeled with combined metabolic labeling, indicating that this strategy may provide a valuable tool for investigating the communication, competition, and cooperation within a microbial ecosystem.[33]

In order to intuitively observe the RGB fluorescence of samples, we then fabricated a portable spectrometer with three tunable band-pass filters (blue, green, and red optical filters) by using 3D printing technology (Fig. S3†).[34] A commercialized mobile application (App) on a smartphone was further used for conveniently and directly reading the RGB fluorescence values of the samples by connecting it to the portable spectrometer (Fig. 3A and B). When the samples are labeled by modified metabolites and then analyzed by this portable spectrometer, the color of the fluorescence emitted by the sample can be observed under excitation with a portable flashlight. The RGB fluorescence values of the samples can be directly read with the App through the filters at three specific wavelengths (coined the "Microcolor system"), and this provides great convenience for detection of the fluorescent samples.

In order to verify that the Microcolor system will provide a direct readout of RGB values, the RGB fluorescence of these metabolite derivatives was tested. When these RGB fluorescent metabolites were mixed in different proportions, a characteristic fluorescence emission was observed by the Microcolor system (Fig. 3C). Then, the Microcolor system was used for identifying various evolutionarily distant bacterial species. Eight bacterial species, consisting of *Bacillus thuringiensis*, *B. subtilis*, *E. coli*, *Clostridium difficile*, *Clostridium butyricum*, *Peptostreptococcus anaerobius*, *S. aureus*, and *E. faecalis*, were all labeled by RGB fluorescent metabolites and detected by the Microcolor system. As expected, after being cultured with RGB probes, each bacterial species displayed a specific fluorescent profile with distinguishing RGB values that matched with the fluorescence spectra of the bacteria (Fig. 3D). Fluorescence imaging was also used to confirm the validity of the Microcolor system in identifying the bacteria, and was found to be consistent with the result measured by the Microcolor system (Fig. S4†). Furthermore, the RGB values produced by the App were further analyzed by principal component analysis (PCA).[35] Fig. 3E reveals that the analysis achieved a meaningful classification of bacterial species based on their unique fluorescent fingerprints. These results indicated that the Microcolor system effectively and conveniently distinguished between bacterial species and might be a useful tool for bacterial detection.

After demonstrating that the Microcolor system can identify between bacterial species *in vitro*, we further explored whether this system can detect bacterial species in complex environments. First, the emission of two pathogenic bacteria, *E. coli* and *S. aureus*, was tested by the Microcolor system. A blue and

pink color was observed for *E. coli* and *S. aureus*, respectively, which coincided with the results of the fluorescence spectra and fluorescence imaging (Fig. 4A). Accordingly, a mixture of the two bacteria displayed an overlay of the two colors appearing as a white color, which was the same as that of the fluorescence spectra. Interestingly, when the mixture of the two bacteria was treated with piperacillin (one of the most effective antibiotics against *E. coli*)[36] and analyzed by the Microcolor system, the blue color of *E. coli* almost disappeared, and the color of the mixture changed to the pink color previously shown by *S. aureus*. Similarly, after being treated with cloxacillin (a narrow-spectrum antibiotic for *S. aureus* infection),[37] the mixture exhibited a color change from white to blue. The same results were also obtained *via* fluorescence spectra and fluorescence imaging (Fig. 4A and S5†). These results demonstrated that the Microcolor system was able to distinguish different bacterial species in mixed culture.

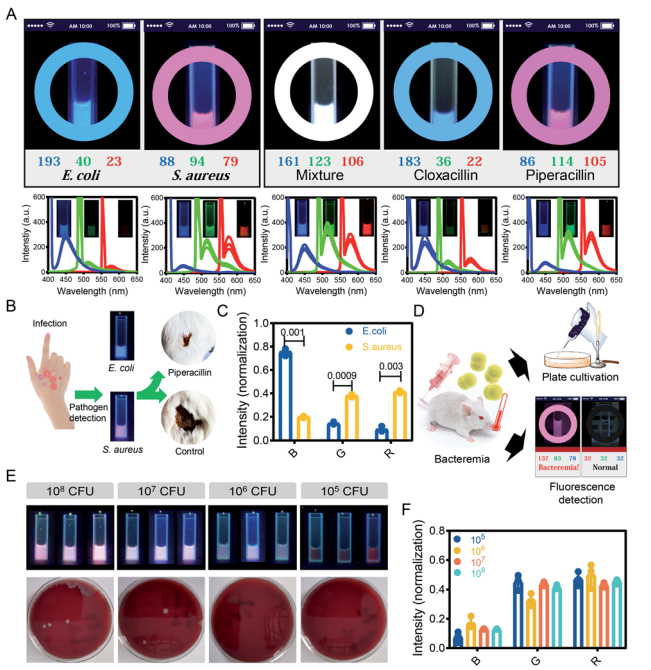

Fig. 4 The labeling and detection of bacteria in complex environments by the Microcolor system. (A) Microcolor system detection of *E. coli*, *S. aureus*, a mixture of *E. coli* and *S. aureus*, and the mixture after treatment with Piperacillin and cloxacillin. Piperacillin and cloxacillin were used to kill *E. coli* and *S. aureus*, respectively. A representative image of three biological replicates is shown. (B) Microcolor system for identifying pathogenic bacterium infecting mouse skin. The mice that received Microcolor system-guided antimicrobial treatment exhibited rapid wound healing. (C) Quantitative analysis of the RGB values detected by the Microcolor system in infected mouse skin. Typical data from at least three independent repeated experiments are presented. (D) A schematic diagram showing how the Microcolor system diagnoses bacteremia. As compared with the blood culture method, the Microcolor system showed significant superiority in terms of both speed and detection limit. (E) Comparison of the Microcolor system and the blood culture method for detecting different levels of bacteremia in a mouse model. Three biological replicates are shown. (F) Quantitative analysis of the RGB values detected by the Microcolor system in a mouse bacteremia model.

Here, the Microcolor system was applied to detect bacterial infection in murine skin infection and bacteremia models.[38] *E. coli*- and *S. aureus*-mediated skin infection models were established using mice, and pus samples were collected from infected mice and further analyzed by the Microcolor system. After labeling and analysis by the Microcolor system, the pathogenic bacteria were identified by comparing their emitted color with the pre-established fluorescent fingerprint data (Fig. 4B, C and S6†). The identification of pathogens is an essential prerequisite for the rational and correct use of antibiotics. Benefiting from the guidance of the Microcolor system, the mice receiving symptomatic antimicrobial therapy displayed accelerated wound closures (65.4% of mice treated with antimicrobial therapy *versus* 18.1% of untreated mice). Because the entire process was carried out in a bacterial culture medium, the cellular components from the human body in the samples might not affect this method.

Bacteremia is a dangerous disease associated with severe mortality. Clinically, detection based on blood culture takes up to 2 days, and this may delay antimicrobial treatments.[39] *S. aureus*-mediated bacteremia models were established using mice, and blood samples were collected from mice with bacteremia and further analyzed by the Microcolor system. As shown in Fig. 4D, the Microcolor system accurately diagnosed *S. aureus*-mediated bacteremia in whole-blood samples within 12 h. As compared with the blood culture method, our method achieved a relatively low detection limit. Specifically, the Microcolor system detected bacteremia with 10^5 colony-forming units (CFU) of *S. aureus* per mouse. In sharp contrast, even at an injection dose of 10^7 CFU, the blood culture method still exhibited a false negative result (Fig. 4E). The RGB values detected by the Microcolor system in mouse bacteremia models were further normalized and analyzed, and there was no significant difference between mice infected with different bacterial concentrations (Fig. 4F and S7†). Through the above research, the Microcolor system was proven to detect bacteria in samples from living organisms, indicating that the Microcolor system possesses the potential to diagnose diseases that are accompanied by changes in bacterial fingerprints in a complex environment. With the capacity to innocuously label each species of bacteria in a complex environment, the Microcolor system might be able to identify unique microbiota consisting of different proportions of bacteria.

To verify whether the Microcolor system can diagnose diseases by identifying the structure of the microbiota, we implemented a proof-of-principle study to evaluate its clinical utility. Head and neck squamous cell carcinoma (HNSCC) is one of the most common cancer types worldwide. OSCC, as one of the key members of HNSCC, has been reported to have a close relationship with oral microbiota alterations.[40,41] Indeed, bacteria including *Capnocytophaga gingivalis*, *Prevotella melaninogenica*, and *Streptococcus mitis* have been recognized as important markers for the early diagnosis of OSCC.[9]

In this study, saliva samples from healthy volunteers (n = 10), OSCC patients (n = 29), and patients with precancerous lesions (n = 10) were collected and analyzed by the Microcolor system (Fig. 5A). Saliva samples from 5 healthy volunteers and 5

OSCC patients were initially used to establish the mathematical modeling (Fig. S8†). As shown in Fig. 5B, the fluorescence patterns between these two groups displayed obvious differences. Strong red fluorescence was found in saliva samples from all 5 OSCC patients. In contrast, enhanced green fluorescence was only observed in 2 OSCC cases. Overall, the comprehensive consideration of RGB values enabled the accurate identification of cancerous cases. The fluorescent fingerprints of saliva from healthy individuals varied from each other. However, OSCC cases showed a similar fluorescence pattern. This result was also confirmed by PCA analysis (Fig. 5C). Although it is obvious that saliva samples from healthy people and OSCC patients were significantly different, a quantitative criterion is still required for the diagnosis.

We further developed a logistic regression model that connected RGB values to the different types of cases.[42] A regression equation for use with the Microcolor system that would optimally predict the risk of developing OSCC is listed in Fig. 5D. In this regression model, the more negative the result, the higher the probability of a OSCC diagnosis. Additionally, it was noted that red fluorescence accounted for a much larger proportion of the result than the other variables included in the model. This regression equation was used to predict the state of 24 other samples (Fig. 5E and S9†). By using a threshold value of 0, 23 of 24 patients were successfully identified as having OSCC, and this result led to a relatively high accuracy rate of 95.8%. Only one false negative result was obtained during this small-scale investigation.

To verify the effectiveness of the Microcolor system for OSCC prediction, the change in the oral microbiome between OSCC patients and healthy people was measured with polymerase chain reaction (PCR) technology. As shown in Fig. S10,† significantly increased *Streptococcus* and *Prevotella*, which are the important markers for OSCC, were observed in the oral microbiome of OSCC patients. This result indicated that the Microcolor system is an effective approach for OSCC diagnosis. Precancerous lesions at the early stage may be misdiagnosed as cancers before they progress to OSCC.[43] To address this issue, we also tested whether this logistic regression model could distinguish between the saliva samples from patients with OSCC or precancerous lesions (Fig. S11†). As shown in Fig. 5D and E, most patient samples of precancerous lesions or benign tumors (10 of 10) displayed an emission color that was similar to that of healthy volunteers. In consistence with morphological observation, the logistic regression model also suggested that the lesions of these 10 patients were unlikely to be malignant tumors.

These results demonstrated that the Microcolor system is an effective approach for OSCC diagnosis. This method might be further developed so that it can provide valuable guidance for cancer screening.

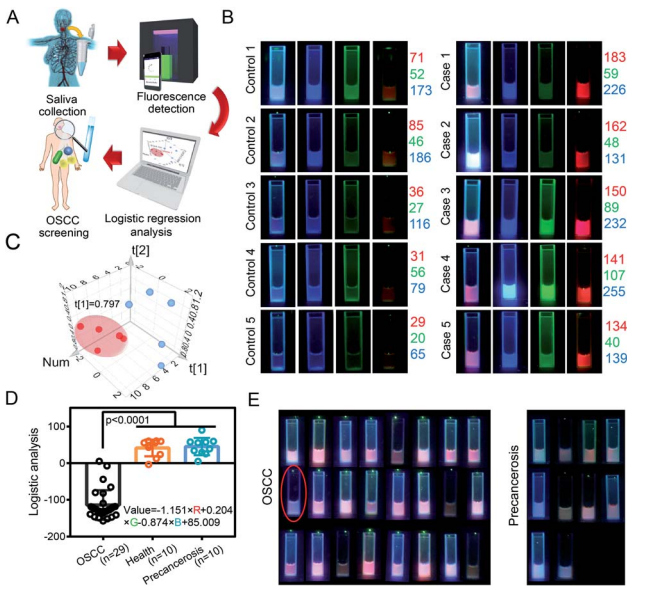

Fig. 5 Diagnosis of OSCC from human saliva samples. (A) A schematic diagram showing the clinical application of the Microcolor system. (B) Fluorescence fingerprints of saliva samples from 5 clinical OSCC cases and 5 healthy individuals. (C) PCA analysis of the fluorescence fingerprints in saliva samples from 5 clinical OSCC cases (red dots) and 5 healthy individuals (blue dots). (D) Formula obtained from logistic regression to distinguish the saliva samples of OSCC cases from precancerous cases/healthy individuals; 28 of 29 (96.5%) OSCC cases were detected. Statistical significance was calculated *via* one-way analysis of variance (ANOVA) with a Tukey *post hoc* test. (E) Fluorescence fingerprints of saliva samples from 24 clinical OSCC cases and 10 precancerous cases. False-positive samples are circled. The mean values and standard deviations (S.D.) of at least three independent experiments are presented.

Conclusions

In this study, we have proposed a method based on pattern recognition for diagnosing diseases that are accompanied by changes in the microbiota structure. Three bioorthogonal metabolites, B-Ala, G-Glu, and R-Gal, were synthesized. Based on the fact that metabolites are incorporated into bacteria through biosynthetic pathways, these metabolites are utilized differently by different types of bacteria. Thus, different bacteria will exhibit characteristic RGB fluorescence emission and produce a unique and distinguishable true color pattern. By combining this method with different detection methods, such as portable spectrometry, fluorescence spectrophotometry, flow cytometry, and fluorescence microscopy, there is the potential for this method to be flexibly used for various medical applications. It can be expected that the combination of the Microcolor system and other clinical technologies might lead to an update of the current methods for studying host–microbial interactions and disease diagnosis.

Ethical statement

All animal studies were approved by the Institutional Animal Care and Use Committee (IACUC) of the Animal Experiment Center of Wuhan University (Wuhan, China). All mouse experimental procedures were performed in accordance with the Regulations for the Administration of Affairs Concerning Experimental Animals approved by the State Council of the People's Republic of China.

Saliva samples were obtained from patients at the School and Hospital of Stomatology of Wuhan University. The School and Hospital of Stomatology of Wuhan University Medical Ethics Committee approved this study, and informed consent was obtained from the patients before they underwent surgery. The clinical stages of their HNSCC were classified according to the guidelines of the International Union Against Cancer (UICC 2002).

Conflicts of interest

There are no conflicts to declare.

Acknowledgements

This work was supported by the National Key Research and Development Program of China (2019YFA0905603) and the National Natural Science Foundation of China (51690152, 21721005 and 51833007).

Notes and references

1 K. Z. Coyte, J. Schluter and K. R. Foster, *Science*, 2015, **350**, 663.
2 J. A. Gilbert, R. A. Quinn, J. Debelius, Z. Z. Xu, J. Morton, N. Garg, J. K. Jansson, P. C. Dorrestein and R. Knight, *Nature*, 2016, **535**, 94.
3 S. V. Lynch and O. Pedersen, *N. Engl. J. Med.*, 2016, **375**, 2369–2379.
4 M. O. Din, T. Danino, A. Prindle, M. Skalak, J. Selimkhanov, K. Allen, E. Julio, E. Atolia, L. S. Tsimring, S. N. Bhatia and J. Hasty, *Nature*, 2016, **536**, 81.
5 O. Felfoul, M. Mohammadi, S. Taherkhani, D. de Lanauze, Y. Zhong Xu, D. Loghin, S. Essa, S. Jancik, D. Houle, M. Lafleur, L. Gaboury, M. Tabrizian, N. Kaou, M. Atkin, T. Vuong, G. Batist, N. Beauchemin, D. Radzioch and S. Martel, *Nat. Nanotechnol.*, 2016, **11**, 941.
6 D.-W. Zheng, Y. Chen, Z.-H. Li, L. Xu, C.-X. Li, B. Li, J.-X. Fan, S.-X. Cheng and X.-Z. Zhang, *Nat. Commun.*, 2018, **9**, 1680.
7 J.-X. Fan, Z.-H. Li, X.-H. Liu, D.-W. Zheng, Y. Chen and X.-Z. Zhang, *Nano Lett.*, 2018, **18**, 2373–2380.
8 D.-W. Zheng, X. Dong, P. Pan, K.-W. Chen, J.-X. Fan, S.-X. Cheng and X.-Z. Zhang, *Nat. Biomed. Eng.*, 2019, **3**, 717–728.
9 D. L. Mager, A. D. Haffajee, P. M. Devlin, C. M. Norris, M. R. Posner and J. M. Goodson, *J. Transl. Med.*, 2005, **3**, 27.
10 A. M. Thomas, P. Manghi, F. Asnicar, E. Pasolli, F. Armanini, M. Zolfo, F. Beghini, S. Manara, N. Karcher, C. Pozzi, S. Gandini, D. Serrano, S. Tarallo, A. Francavilla, G. Gallo, M. Trompetto, G. Ferrero, S. Mizutani, H. Shiroma, S. Shiba, T. Shibata, S. Yachida, T. Yamada, J. Wirbel, P. Schrotz-King, C. M. Ulrich, H. Brenner, M. Arumugam, P. Bork, G. Zeller, F. Cordero, E. Dias-Neto, J. C. Setubal, A. Tett, B. Pardini, M. Rescigno, L. Waldron, A. Naccarati and N. Segata, *Nat. Med.*, 2019, **25**, 667–678.
11 J. Wirbel, P. T. Pyl, E. Kartal, K. Zych, A. Kashani, A. Milanese, J. S. Fleck, A. Y. Voigt, A. Palleja, R. Ponnudurai, S. Sunagawa, L. P. Coelho, P. Schrotz-King, E. Vogtmann, N. Habermann, E. Niméus, A. M. Thomas, P. Manghi, S. Gandini, D. Serrano, S. Mizutani, H. Shiroma, S. Shiba, T. Shibata, S. Yachida, T. Yamada, L. Waldron, A. Naccarati, N. Segata, R. Sinha, C. M. Ulrich, H. Brenner, M. Arumugam, P. Bork and G. Zeller, *Nat. Med.*, 2019, **25**, 679–689.
12 M. S. Shah, T. Z. DeSantis, T. Weinmaier, P. J. McMurdie, J. L. Cope, A. Altrichter, J.-M. Yamal and E. B. Hollister, *Gut*, 2018, **67**, 882.
13 H. J. Chung, C. M. Castro, H. Im, H. Lee and R. Weissleder, *Nat. Nanotechnol.*, 2013, **8**, 369.
14 S. Sauer and M. Kliem, *Nat. Rev. Microbiol.*, 2010, **8**, 74.
15 J. Kuczynski, C. L. Lauber, W. A. Walters, L. W. Parfrey, J. C. Clemente, D. Gevers and R. Knight, *Nat. Rev. Genet.*, 2011, **13**, 47.
16 F. Natalio, R. Fuchs, S. R. Cohen, G. Leitus, G. Fritz-Popovski, O. Paris, M. Kappl and H.-J. Butt, *Science*, 2017, **357**, 1118.
17 A. D. Radkov, Y.-P. Hsu, G. Booher and M. S. VanNieuwenhze, *Annu. Rev. Biochem.*, 2018, **87**, 991–1014.
18 H. Wang, R. Wang, K. Cai, H. He, Y. Liu, J. Yen, Z. Wang, M. Xu, Y. Sun, X. Zhou, Q. Yin, L. Tang, I. T. Dobrucki, L. W. Dobrucki, E. J. Chaney, S. A. Boppart, T. M. Fan, S. Lezmi, X. Chen, L. Yin and J. Cheng, *Nat. Chem. Biol.*, 2017, **13**, 415.
19 H. Lam, D.-C. Oh, F. Cava, C. N. Takacs, J. Clardy, M. A. de Pedro and M. K. Waldor, *Science*, 2009, **325**, 1552.
20 D. K. Ranjit and K. D. Young, *J. Bacteriol.*, 2013, **195**, 2452.
21 E. Kuru, C. Lambert, J. Rittichier, R. Till, A. Ducret, A. Derouaux, J. Gray, J. Biboy, W. Vollmer, M. VanNieuwenhze, Y. V. Brun and R. E. Sockett, *Nat. Microbiol.*, 2017, **2**, 1648–1657.
22 Y.-P. Hsu, E. Hall, G. Booher, B. Murphy, A. D. Radkov, J. Yablonowski, C. Mulcahey, L. Alvarez, F. Cava, Y. V. Brun, E. Kuru and M. S. VanNieuwenhze, *Nat. Chem.*, 2019, **11**, 335–341.
23 C. Jiang, P. J. B. Brown, A. Ducret and Y. V. Brun, *Nature*, 2014, **506**, 489.
24 G. W. Liechti, E. Kuru, E. Hall, A. Kalinda, Y. V. Brun, M. VanNieuwenhze and A. T. Maurelli, *Nature*, 2013, **506**, 507.
25 S. E. Pidgeon, J. M. Fura, W. Leon, M. Birabaharan, D. Vezenov and M. M. Pires, *Angew. Chem., Int. Ed.*, 2015, **54**, 6158–6162.
26 E. Kuru, H. V. Hughes, P. J. Brown, E. Hall, S. Tekkam, F. Cava, M. A. de Pedro, Y. V. Brun and M. S. VanNieuwenhze, *Angew. Chem., Int. Ed.*, 2012, **51**, 12519–12523.
27 W. Wang, L. Lin, Y. Du, Y. Song, X. Peng, X. Chen and C. J. Yang, *Nat. Commun.*, 2019, **10**, 1317.
28 P. J. Calabretta, H. L. Hodges, M. B. Kraft, V. M. Marando and L. L. Kiessling, *J. Am. Chem. Soc.*, 2019, **141**, 9262–9272.
29 R. Sadamoto, T. Matsubayashi, M. Shimizu, T. Ueda, S. Koshida, T. Koda and S.-I. Nishimura, *Chem.–Eur. J.*, 2008, **14**, 10192–10195.
30 K. E. DeMeester, H. Liang, M. R. Jensen, Z. S. Jones, E. A. D'Ambrosio, S. L. Scinto, J. Zhou and C. L. Grimes, *J. Am. Chem. Soc.*, 2018, **140**, 9458–9465.

31 A. Dumont, A. Malleron, M. Awwad, S. Dukan and B. Vauzeilles, *Angew. Chem., Int. Ed.*, 2012, **51**, 3143–3146.
32 J. E. Kwon, S. Park and S. Y. Park, *J. Am. Chem. Soc.*, 2013, **135**, 11239–11246.
33 S. R. Scott, M. O. Din, P. Bittihn, L. Xiong, L. S. Tsimring and J. Hasty, *Nat. Microbiol.*, 2017, **2**, 17083.
34 K. Pardee, S. Slomovic, P. Q. Nguyen, J. W. Lee, N. Donghia, D. Burrill, T. Ferrante, F. R. McSorley, Y. Furuta, A. Vernet, M. Lewandowski, C. N. Boddy, N. S. Joshi and J. J. Collins, *Cell*, 2016, **167**, 248–259.
35 J. W. Lee, J.-S. Lee and Y.-T. Chang, *Angew. Chem., Int. Ed.*, 2006, **45**, 6485–6487.
36 P. N. A. Harris, P. A. Tambyah, D. C. Lye, Y. Mo, T. H. Lee, M. Yilmaz, T. H. Alenazi, Y. Arabi, M. Falcone, M. Bassetti, E. Righi, B. A. Rogers, S. Kanj, H. Bhally, J. Iredell, M. Mendelson, T. H. Boyles, D. Looke, S. Miyakis, G. Walls, M. Al Khamis, A. Zikri, A. Crowe, P. Ingram, N. Daneman, P. Griffin, E. Athan, P. Lorenc, P. Baker, L. Roberts, S. A. Beatson, A. Y. Peleg, T. Harris-Brown and D. L. Paterson, *J. Am. Med. Assoc.*, 2018, **320**, 984–994.
37 P. M. Colavite, L. L. W. Ishikawa, S. F. G. Zorzella-Pezavento, L. R. C. d. Oliveira, T. G. D. França, L. C. da Rosa, F. Chiuso-Minicucci, A. E. Vieira, C. F. Francisconi, M. d. L. R. d. S. da Cunha, G. P. Garlet and A. Sartori, *Cell. Microbiol.*, 2016, **18**, 998–1008.
38 C. Mao, Y. Xiang, X. Liu, Z. Cui, X. Yang, K. W. K. Yeung, H. Pan, X. Wang, P. K. Chu and S. Wu, *ACS Nano*, 2017, **11**, 9010–9021.
39 A. Pechorsky, Y. Nitzan and T. Lazarovitch, *J. Microbiol. Methods*, 2009, **78**, 325–330.
40 L. Rao, L.-L. Bu, L. Ma, W. Wang, H. Liu, D. Wan, J.-F. Liu, A. Li, S.-S. Guo, L. Zhang, W.-F. Zhang, X.-Z. Zhao, Z.-J. Sun and W. Liu, *Angew. Chem., Int. Ed.*, 2018, **130**, 998–1003.
41 L. Mao, W. K. Hong and V. A. Papadimitrakopoulou, *Cancer Cell*, 2004, **5**, 311–316.
42 K. G. Shah, V. Singh, P. C. Kauffman, K. Abe and P. Yager, *Anal. Chem.*, 2018, **90**, 6967–6974.
43 B. W. Neville and T. A. Day, *Ca-Cancer J. Clin.*, 2002, **52**, 195–215.